Cucurbit[8]uril Mediated Donor-Acceptor Ternary Complexes: A Model System for Studying Charge-Transfer Interactions

Frank Biedermann and Oren A. Scherman

Melville Laboratory for Polymer Synthesis, Department of Chemistry, University of Cambridge,
Lensfield Road, Cambridge, CB2 1EW, United Kingdom

E-mail: oas23@cam.ac.uk

1   General considerations

Methyl viologen dichloride was purchased from Sigma Aldrich. CB[8] was prepared according to literature procedure[§] ^{1}H and ^{13}C NMR data were collected on a Bruker Avance 500 BB-ATM spectrometer. Chemical shifts (δ) are reported in ppm. UV/vis spectra were recorded using a Varian Cary 4000 UV/vis spectrophotometer in aqueous solutions with 0.1 nm resolution at 25°C. High-resolution ESI mass spectra were obtained from a LTQ Orbitrap Velos system. Isothermal titration experiments were carried out on a ITC200 from Microcal, Inc. at 25°C in water.

2   Synthesis and Characterisation of the aryl-viologens

The aryl-viologens were synthesized in analogy to literature procedures starting from 1,1'-bis(2,4-dinitrophenyl)-[4,4'-bipyridine]-1,1'-diium dichloride:[†]

Typical procedure: A solution of 1,1'-bis(2,4-dinitrophenyl)-[4,4'-bipyridine]-1,1'-diium dichloride (0.5 g, 1.6 mmol) and three equivalents corresponding substituted aniline (e.g. 4-bromo-aniline for the synthesis of V-Br) were refluxed in 250 mL ethanol. The reaction progress can be followed by ^{1}H-NMR and by ESI-MS. The reaction reaches completion with electron-pushing substituents (such as methyl-) in less then 24 hours whereas for electron-withdrawing substituents several days are required. Upon full conversion, the solution was concentrated to approx. 100 mL under reduced pressure and poured into 750 mL of THF. The precipitate was collected after 2 hours by suction filtration and washed with THF (ca 100 mL). The solid was redissolved in a minimum amount of ethanol with heating and re-precipitated into THF. The solid was dried in a vacuum-oven overnight at 40°C to gain the aryl-viologen in typically 60-85% yield.

1,1'-diphenyl-[4,4'-bipyridine]-1,1'-diium dichloride (**V-H**):
^{1}H NMR (500 MHz, D$_2$O): δ = 9.44 (d, 4H, 7.0 Hz), 8.83 (d, 4H, 7.0 Hz), 7.87-7.81 (m, 10H) ppm; ^{13}C NMR (125 MHz, D$_2$O): δ = 150.5, 145.5, 142.2, 132.0, 130.6, 127.0, 124.0 ppm. ESI-MS: [M^{2+}]: expected 155.0735, found 155.0743.

[§] Kim, J.; Jung, I. S.; Kim, S. Y.; Lee, E.; Kang, J. K.; Sakamoto, S.; Yamaguchi, K.; Kim, K. J. Am. Chem. Soc. 2000, 122, 540.

[†] Bongard, D.; Möller, M.; Rao, S. N.; Corr, D.; Walder, L. Helv. Chim. Acta 2005, 88, 3200 3209.

1,1'-di-*p*-tolyl-[4,4'-bipyridine]-1,1'-diium dichloride (**V-Me**):
^{1}H NMR (500 MHz, D$_2$O): δ = 9.40 (d, 4H, 7.0 Hz), 8.79 (d, 4H, 7.0 Hz), 7.73 (d, 4H, 8.4 Hz), 7.62 (d, 4H, 8.4 Hz), 2.52 (s, 6H) ppm; ^{13}C NMR (125 MHz, D$_2$O): δ = 150.6, 145.7, 143.6, 140.3, 131.4, 127.3, 124.1, 20.7 ppm.
ESI-MS: [M^{2+}]: expected 169.0892, found 169.0898.

1,1'-bis(4-cyanophenyl)-[4,4'-bipyridine]-1,1'-diium dichloride (**V-CN**):
^{1}H NMR (500 MHz, D$_2$O): δ = 9.51 (d, 4H, 6.6 Hz), 8.89 (d, 4H, 6.6 Hz), 8.22 (d, 4H, 8.5 Hz), 8.08 (d, 4H, 8.5 Hz) ppm; ^{13}C NMR (125 MHz, D$_2$O): δ = 151.2, 145.6, 145.0, 134.9, 127.3, 125.3, 117.7, 115.1 ppm.
ESI-MS: [M^{2+}]: expected 180.0688, found 180.0700.

1,1'-bis(4-(ethoxycarbonyl)phenyl)-[4,4'-bipyridine]-1,1'-diium dichloride (**V-CO$_2$Et**):
^{1}H NMR (500 MHz, D$_2$O): δ = 9.48 (d, 4H, 7.1 Hz), 8.82 (d, 4H, 7.1 Hz), 8.37 (d, 4H, 8.9 Hz), 7.97 (d, 4H, 8.9 Hz), 4.47 (q, 4H, 7.2 Hz), 1.41 (t, 6H, 7.2 Hz) ppm; ^{13}C NMR (125 MHz, D$_2$O): δ = 167.1, 151.0, 145.5, 145.2 133.3, 131.6, 127.2, 124.6, 62.9, 13.3 ppm.
ESI-MS: [M^{2+}]: expected 227.0941, found 227.0937.

1,1'-bis(4-aminophenyl)-[4,4'-bipyridine]-1,1'-diium dichloride (**V-NH$_2$**):
^{1}H NMR (500 MHz, D$_2$O): δ = 9.14 (d, 4H, 7.1 Hz), 8.55 (d, 4H, 7.1 Hz), 7.47 (d, 4H, 9.0 Hz), 6.91 (d, 4H, 9.0 Hz) ppm; ^{13}C NMR (125 MHz, D$_2$O): δ = 150.4, 149.2, 144.6, 133.3, 126.7, 125.0, 116.4 ppm.
ESI-MS: [M^{+}]: expected 340.1688, found 340.1666.

1,1'-bis(4-nitrophenyl)-[4,4'-bipyridine]-1,1'-diium dichloride (**V-NO$_2$**):
^{1}H NMR (500 MHz, D$_2$O): δ = 9.57 (d, 4H, 6.5 Hz), 8.93 (d, 4H, 6.5 Hz), 8.68 (d, 4H, 8.7 Hz), 8.18 (d, 4H, 8.7 Hz) ppm; ^{13}C NMR (125 MHz, D$_2$O): δ = 151.4, 149.4, 146.1, 145.7, 127.4, 126.0 ppm.
ESI-MS: [M^{2+}]: expected 200.0586, found 200.0592.

1,1'-bis(4-methoxyphenyl)-[4,4'-bipyridine]-1,1'-diium dichloride (**V-OMe**):
^{1}H NMR (500 MHz, D$_2$O): δ = 9.38 (d, 4H, 7.0 Hz), 8.78 (d, 4H, 7.0 Hz), 7.83 (d, 4H, 9.1 Hz), 7.34 (d, 4H, 9.1 Hz), 4.00 (s, 6H) ppm; ^{13}C NMR (125 MHz, D$_2$O): δ = 161.6, 149.9, 145.1, 135.5, 126.8, 125.5, 115.7, 55.9 ppm.
ESI-MS: [M^{2+}]: expected 185.0841, found 185.0846.

1,1'-bis(4-fluorophenyl)-[4,4'-bipyridine]-1,1'-diium dichloride (**V-F**):
^{1}H NMR (500 MHz, D$_2$O): δ = 9.43 (d, 4H, 6.8 Hz), 8.82 (d, 4H, 6.8 Hz), 7.91 (dd, 4H, 8.6 Hz, 4.5 Hz), 7.55 (t, 4H, 8.6 Hz) ppm; ^{13}C NMR (125 MHz, D$_2$O): δ = 165.2, 163.2, 150.5, 145.6, 138.3, 127.0, 126.5, 126.4, 117.7, 117.5 ppm, ^{19}F NMR (376 MHz, D$_2$O): 108.5 ppm.
ESI-MS: [M^{2+}]: expected 173.0641, found 173.0660.

1,1'-bis(4-chlorophenyl)-[4,4'-bipyridine]-1,1'-diium dichloride (**V-Cl**):
^{1}H NMR (500 MHz, D$_2$O): δ = 9.44 (d, 4H, 6.9 Hz), 8.84 (d, 4H, 6.9 Hz), 7.86 (mc, 8H, 9.0 Hz, 6.6 Hz) ppm; ^{13}C NMR (125 MHz, D$_2$O): δ = 150.6, 145.5, 140.7, 137.8, 130.7, 127.1, 125.6 ppm.
ESI-MS: [M^{2+}]: expected 189.0346, found 189.0354.

1,1'-bis(4-bromophenyl)-[4,4'-bipyridine]-1,1'-diium dichloride (**V-Br**):
^{1}H NMR (500 MHz, D$_2$O): δ = 9.43 (d, 4H, 7.0 Hz), 8.82 (d, 4H, 7.0 Hz), 7.99 (d, 4H,

8.9 Hz), 7.78 (d, 4H, 8.9 Hz) ppm; ^{13}C NMR (125 MHz, D$_2$O): δ = 150.7, 145.4, 141.2, 133.7, 127.1, 126.0, 125.7 ppm.
ESI-MS: [M^{2+}]: expected 233.9830, found 233.9847.

1,1'-bis(4-iodophenyl)-[4,4'-bipyridine]-1,1'-diium dichloride (**V-I**):
^{1}H NMR (500 MHz, D$_2$O): δ = 9.43 (d, 4H, 6.9 Hz), 8.83 (d, 4H, 6.9 Hz), 8.20 (d, 4H, 8.8 Hz), 7.63 (d, 4H, 8.8 Hz) ppm; ^{13}C NMR (125 MHz, D$_2$O): δ = 150.7, 145.3, 141.9, 139.8, 127.1, 125.6, 110.0, 98.1 ppm.
ESI-MS: [M^{2+}]: expected 280.9696, found 280.9691.

3 Supporting Figures
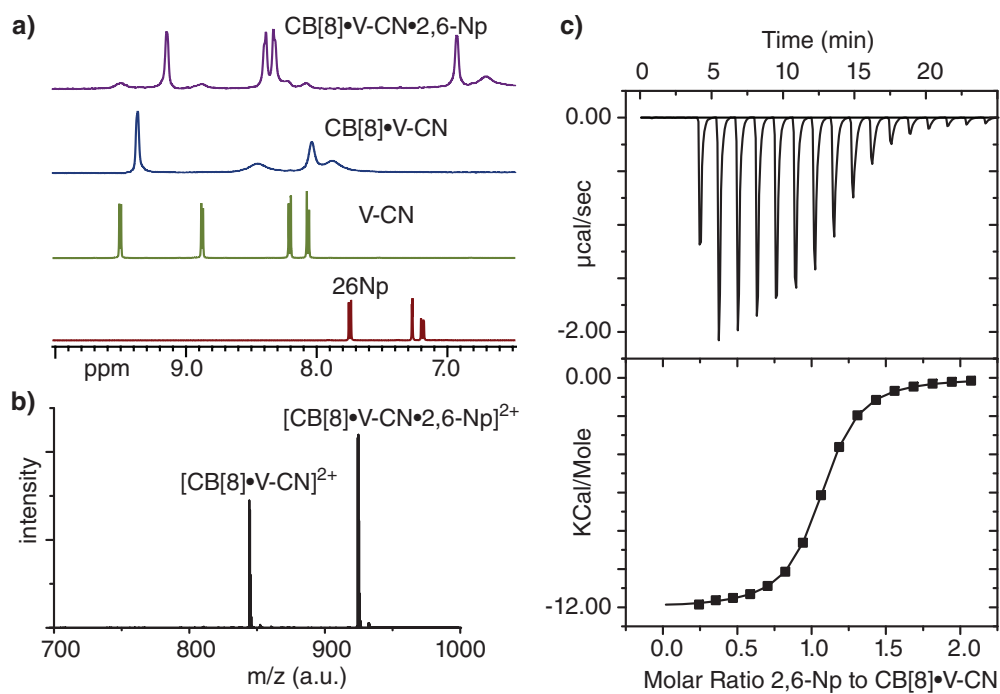
Figure S1: (a) Aromatic region of the ^{1}H NMR spectra in D$_2$O for the ternary complex CB[8]·V-CN·2,6-Np and each of the individual components. (b) FT-ESI-MS spectrum for a 1:1:1 mixture of CB[8], V-CN and 2,6-Np. (c) ITC binding isotherms for the titration of CB[8]·V-CN with 2,6-Np in aqueous solution at 25 °C.

G1	$K_{aq}(1)$ (M^{-1})	$\Delta G_{aq}(1)$ $(kJ\ mol^{-1})$	$\Delta H_{aq}(1)$ $(kJ\ mol^{-1})$	$-T \cdot \Delta S_{aq}(1)$ $(kJ\ mol^{-1})$
V-NO$_2$	$(1.0 \pm 0.3) \times 10^6$	-34.3 ± 0.4	-15.3 ± 0.3	-19.0 ± 0.7
V-CN	$(2.5 \pm 0.3) \times 10^6$	-36.5 ± 0.4	-33.8 ± 0.4	-2.7 ± 0.8
V-CO$_2$Et	$(1.9 \pm 0.3) \times 10^6$	-35.8 ± 0.4	-33.7 ± 0.4	-2.1 ± 0.8
V-H	$(2.9 \pm 0.3) \times 10^6$	-36.8 ± 0.4	-116.5 ± 0.4	79.7 ± 0.8
V-Me	$(2.2 \pm 0.3) \times 10^6$	-36.2 ± 0.4	-85.2 ± 0.4	49.0 ± 0.8
V-OMe	$(3.9 \pm 0.3) \times 10^6$	-37.6 ± 0.4	-112.1 ± 0.4	74.5 ± 0.8
V-NH$_2$	$(6.7 \pm 0.3) \times 10^5$	-33.3 ± 0.4	-69.3 ± 0.4	36.0 ± 0.8
MV	$(1.5 \pm 0.3) \times 10^6$	-35.2 ± 0.4	-27.6 ± 0.4	7.6 ± 0.8

Table 1: Thermodynamic data for the association of the first guest **G1** with CB[8] in H$_2$O at 298 K as determined by ITC.

G1	$K_{aq}(2)$ (M^{-1})	$\Delta G_{aq}(2)$ $(kJ\ mol^{-1})$	$\Delta H_{aq}(2)$ $(kJ\ mol^{-1})$	$-T \cdot \Delta S_{aq}(2)$ $(kJ\ mol^{-1})$
V-CN	$(1.4 \pm 0.3) \times 10^5$	-29.5 ± 0.4	-58.7 ± 0.4	29.2 ± 0.8
V-CO$_2$Et	$(2.2 \pm 0.3) \times 10^5$	-30.5 ± 0.4	-49.5 ± 0.4	19.0 ± 0.8
V-NO$_2$	$(8.1 \pm 0.3) \times 10^4$	-28.0 ± 0.4	-45.4 ± 0.4	17.4 ± 0.8
V-OMe	$(2.5 \pm 0.2) \times 10^3$	-19.4 ± 0.4	$-^a$	$-^a$
V-F	$(1.1 \pm 0.3) \times 10^5$	-28.8 ± 0.4	-54.6 ± 0.5	25.8 ± 0.9
V-Cl	$(1.7 \pm 0.2) \times 10^4$	-24.1 ± 0.3	-42.8 ± 0.4	18.6 ± 0.7

^{a} isotherm is not suitable for accurate fitting of $\Delta H_{aq}(2)$ and $\Delta S_{aq}(2)$.

Table 2: Thermodynamic data for the association of dibenzofuran-functional poly(ethylene glycol) monomethylether (5000 g mol^{-1}) (**DBF-5k-PEG**) with CB[8]·**G1** in H$_2$O at 298 K as determined by ITC. See SI-Figure 4 for the chemical structure of DBF-5k-PEG.
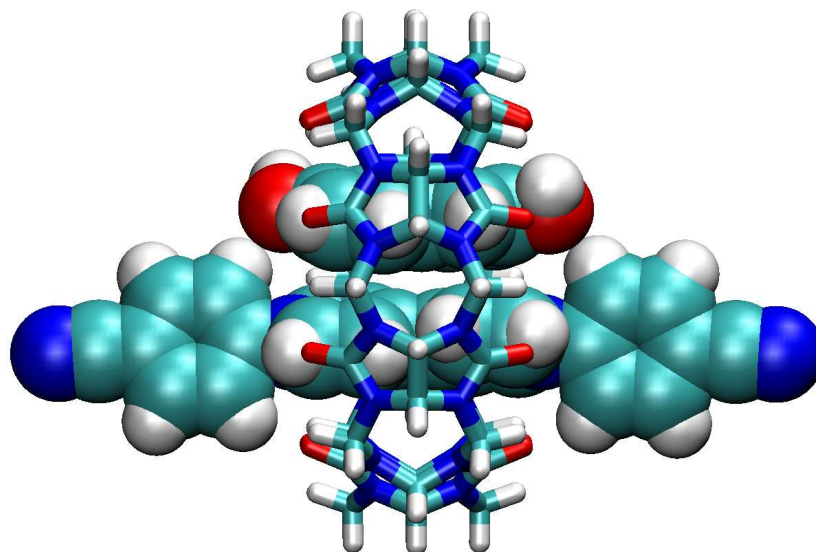
Figure S 2: Geometry optimized structure of the CB[8]·V-CN·2,6-Np ternary complex at DFT-B3LYP/6-31G* level of theory in a vacuum.
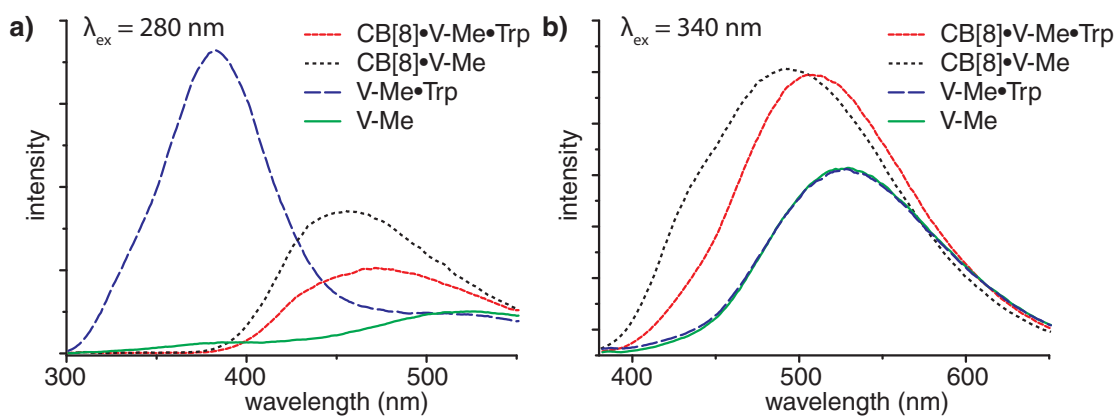
Figure S 3: Fluorescence spetcra at 280 nm excitation (a) and 340 nm excitation (b) for CB[8], **2** and tryptophan (Trp) (50 μM in each component).

G1	CT λ_{max} G2 = 2,6-Np (nm)	CT λ_{max} G2 = 2,7-Np (kJ mol^{-1})
V-OMe	600	-*
V-H	614	460
V-I	623	-*
V-Cl	632	-*
V-F	642	-*
V-CO$_2$Et	646	482
V-CN	660	510
V-NO$_2$	665	503

Table 3: Experimental CT wavelength for ternary CB[8]·acceptor·2,6-Np and CB[8]·acceptor·2,7-Np complexes (0.5 mM in water). * CT wavelength cannot be determined since intra-molecular CT band of acceptor overlaps.
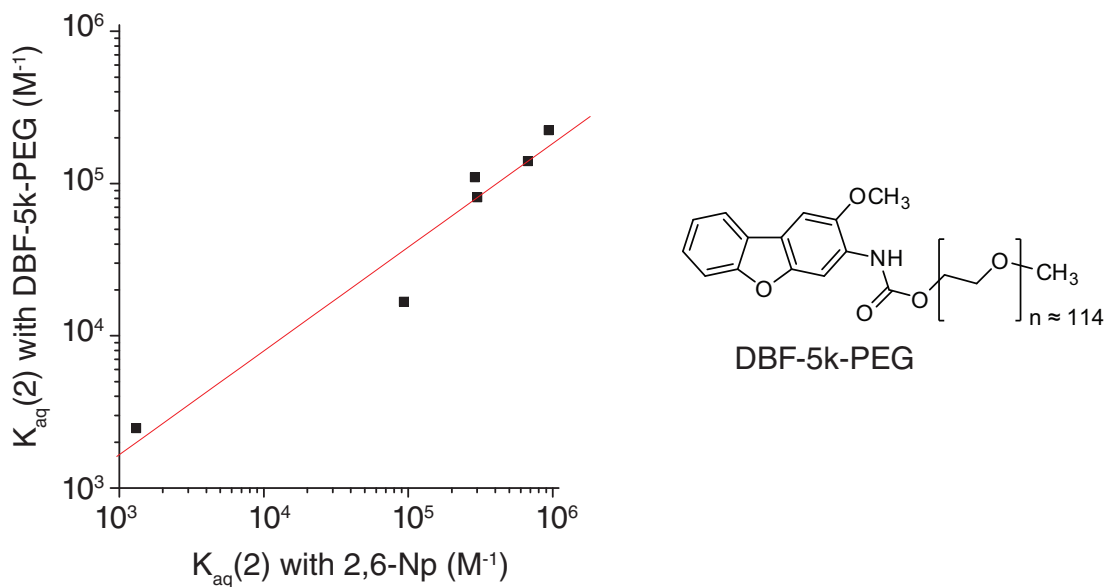
Figure S4: Comparisson of the binding constants $K_{aq}(2)$ for CB[8]·G1 with DBF-5k-PEG-OMe and $K_{aq}(2)$ for CB[8]·G1 with 2,6-Np as determined by ITC in H$_2$O at 298 K.

G2	CT λ_{max} (nm)	E_{HOMO} (kJ mol^{-1})
2-cyanophenol	361	-682.1
4-cyanophenol	365	-675.3
phenol	395	-616.9
4-fluorophenol	396	-622.1
4-chlorophenol	407	-622.9
4-bromophenol	414	-619.9
1,3-dihydroxybenzene	436	-602.4
1,2-dihydroxybenzene	443	-589.8
1,3,5-trihydroxybenzene	444	-607.4
2-methoxybenzene	447	-575.8
2,7-dihydroxynaphthalene	459	-572.4
indole	460	-559.8
3-methoxy-2-naphthol	461	-564.6
2,3-dihydroxynaphthalene	465	-572.0
1,4dihydroxybenzene	473	-568.2
2-naphthol	447	-575.8
4-methoxyphenol	477	-556.7
aniline	481	-561.2
3-aminophenol	485	-557.5
1,4-dimethoxybenzene	488	-546.1
1-naphthol	510	-562.6
sesamol	512	-549.4
1,6-dihydroxynaphthalene	544	-554.4
1,7-dihydroxynaphthalene	554	-548.8
1,5-dihydroxynaphthalene	558	-541.8
6-methoxy-2-naphthol	558	-544.1
2,6-dihydroxynaphthalene	560	-550.3
3-amino-2-methoxy-dibenzofuran	587	-519.5
2-aminoanthracene	656	-503.8

Table 4: Experimentally determined CT λ_{max} for ternary CB[8]·MV·donor complexes (1mM in water) and calculated E_{HOMO} values for the donor in a vacuum at B3LYP/6-311G+** level of theory.
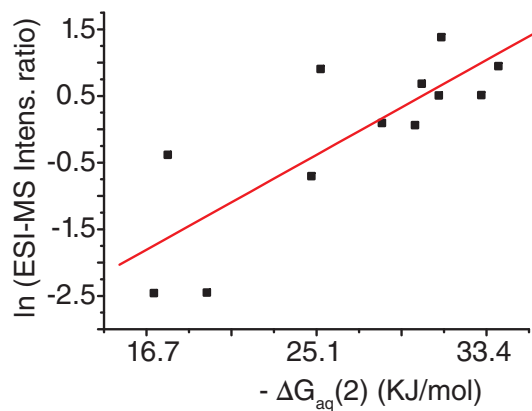
Figure S 5: Correlation of logarithmic ratio of ESI-MS intensities $\ln([CB[8]\cdot G1\cdot 2,6\text{-}Np]\times[CB[8]\cdot G1]^{-1})$ *versus* the measured free Gibbs energy $\Delta G_{aq}(2)$ as obtained by ITC for the series of viologen derivatives V-H - V-I and the second guest 2,6-Np.
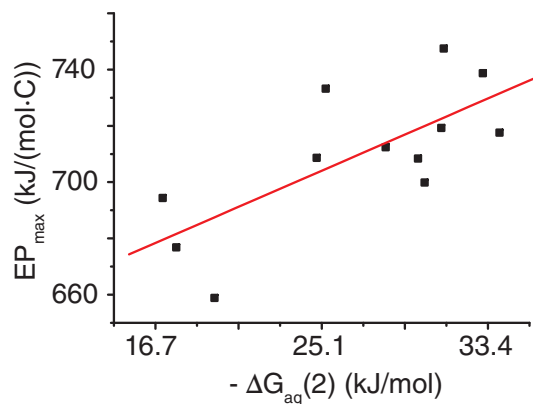
Figure S6: Correlation of the calculated ((B3LYP/6-311G*)) maximum electrostatic potential EP_{max} on the viologen *versus* the measured free Gibbs energy $\Delta G_{aq}(2)$ as obtained by ITC for the series of the aryl viologens and the second guest 2,6-Np.
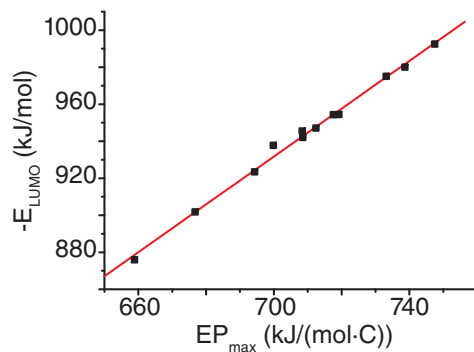
Figure S7: The calculated (B3LYP/6-311G*) E_{LUMO} of the aryl viologens shows an excellent correlation to the maximum electrostatic potential EP_{max} on the viologen unit at the same level of theory.
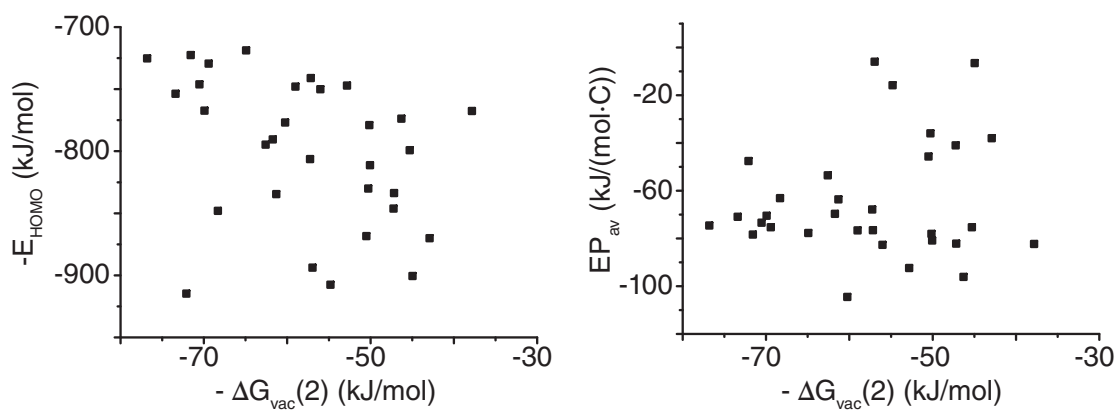
Figure S8: Neither the calculated (B3LYP/6-311G+**) E_{HOMO} nor the average electrostatic potential EP_{av} of the second guest shows a correlation to the calculated free energy $\Delta G_{vac}(2)$ for the ternary complex formation of CB[8]·MV·G2.

4   UV/vis of CB[8]·MV complexes with various donors
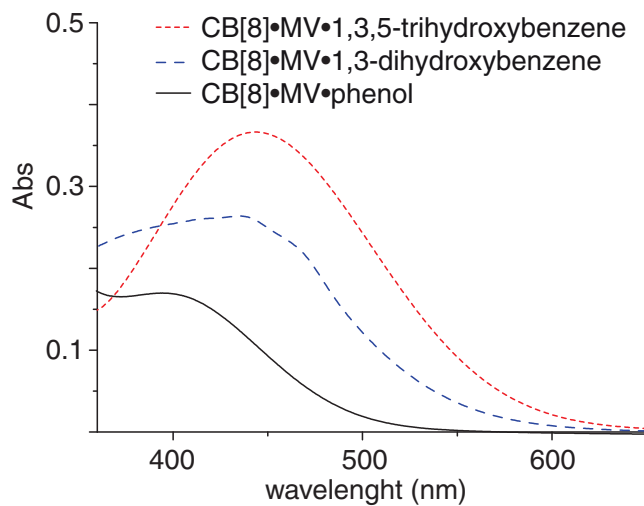
Figure S 9: UV/vis of CB[8]·MV ternary complex with phenol, 1,3-dihydroxyphenol and 1,3,5-trihydroxyphenol (0.5 mM in each component, H_2O).
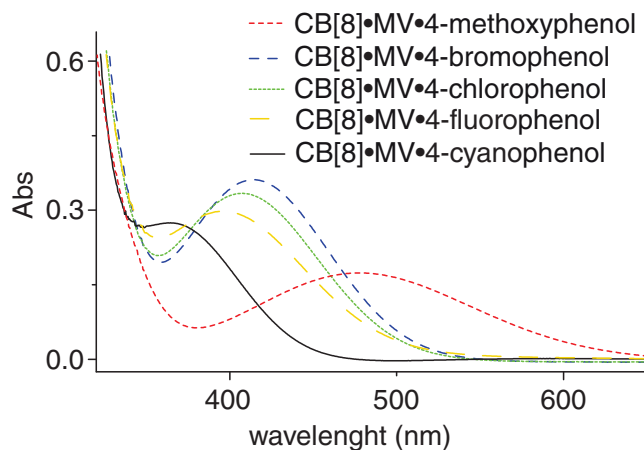
Figure S 10: UV/vis of CB[8]·MV ternary complex with various para-substituted phenols (0.5 mM in each component, H_2O).
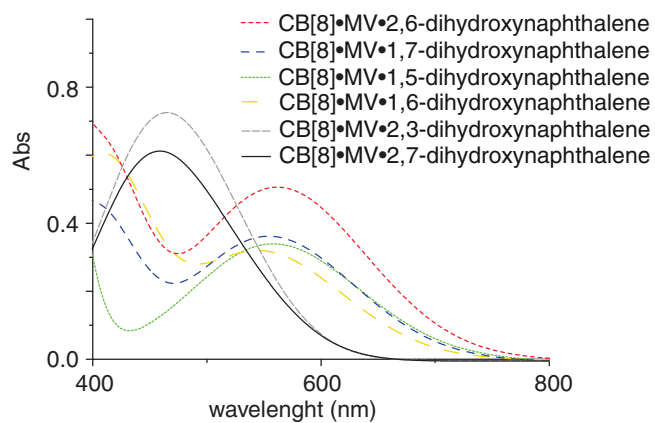
Figure S11: UV/vis of CB[8]·MV ternary complex with regio-isomeric dihydroxynaphthalenes (0.5 mM in each component, H_2O).

5 UV/vis of ternary CB[8]·aryl-viologen complexes with 2,6-Np and 2,7-Np
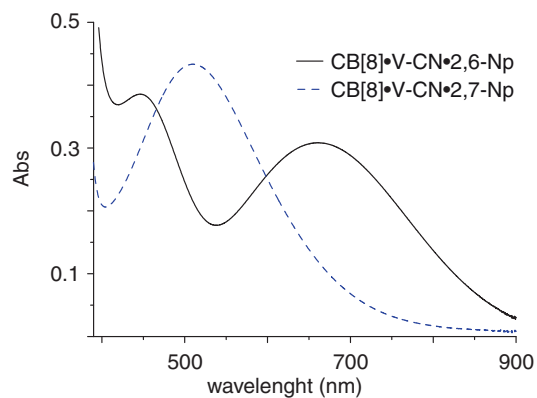
Figure S12: UV/vis of CB[8]·V-CN ternary complex with 2,6-Np and 2,7-Np (0.5 mM in each component, H_2O).
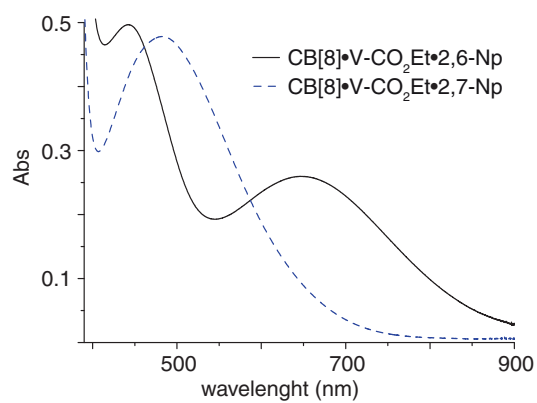
Figure S13: UV/vis of CB[8]·V-CO$_2$Et ternary complex with 2,6-Np and 2,7-Np (0.5 mM in each component, H_2O).
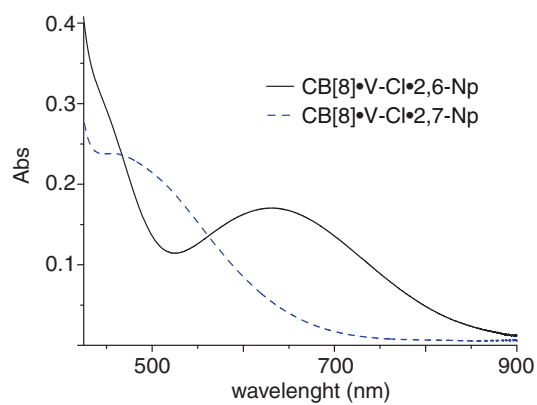
Figure S14: UV/vis of CB[8]·V-Cl ternary complex with 2,6-Np and 2,7-Np (0.5 mM in each component, H_2O).
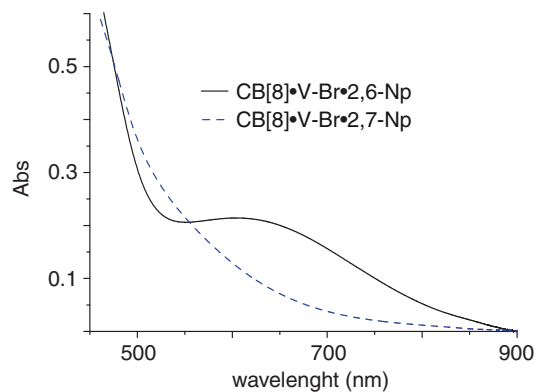
Figure S15: UV/vis of CB[8]·V-Br ternary complex with 2,6-Np and 2,7-Np (0.5 mM in each component, H_2O).
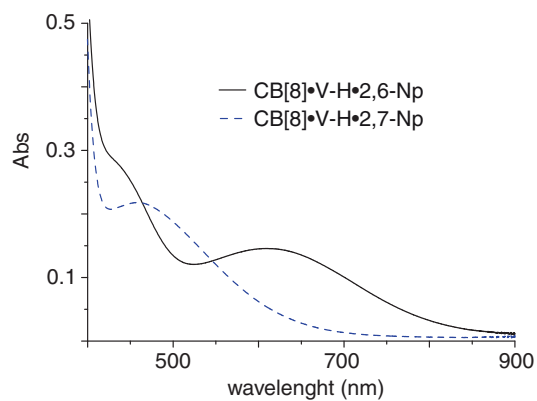
Figure S16: UV/vis of CB[8]·V-H ternary complex with 2,6-Np and 2,7-Np (0.5 mM in each component, H_2O).

14
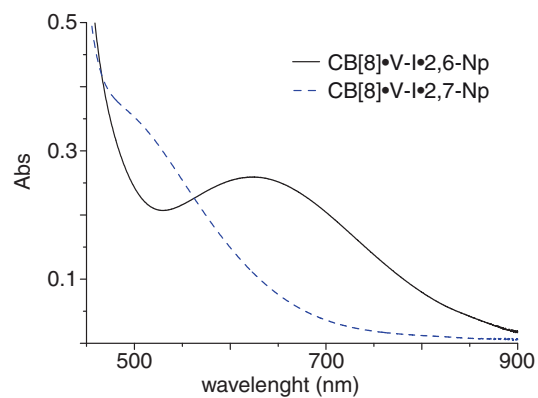
Figure S17: UV/vis of CB[8]·V-I ternary complex with 2,6-Np and 2,7-Np (0.5 mM in each component, H_2O).
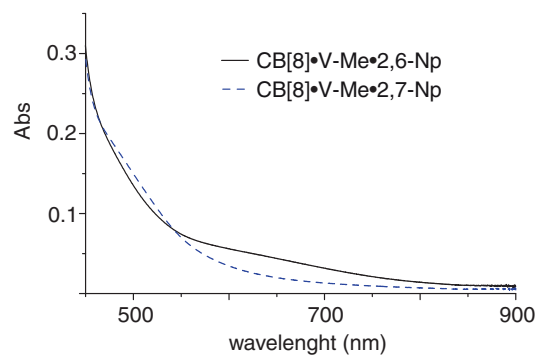
Figure S18: UV/vis of CB[8]·V-Me ternary complex with 2,6-Np and 2,7-Np (0.5 mM in each component, H_2O).
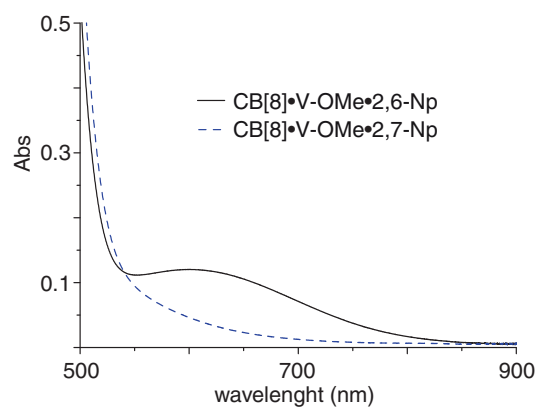
Figure S19: UV/vis of CB[8]·V-OMe ternary complex with 2,6-Np and 2,7-Np (0.5 mM in each component, H_2O).

6   ITC: $K_{aq}(2)$ determination with 2,6-Np
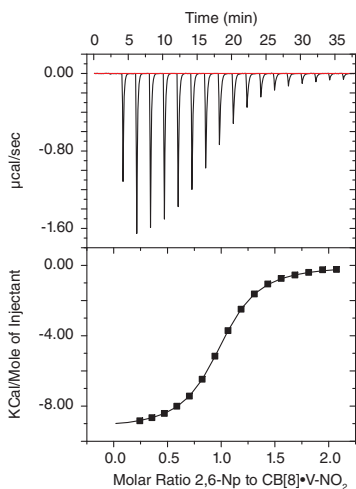
Figure S20: The binding constant of 2,6-Np with CB[8]·V-NO$_2$ was determined by ITC to be (3.0 ± 0.3) x 10^5 M^{-1} in aqueous solution at 298 K.
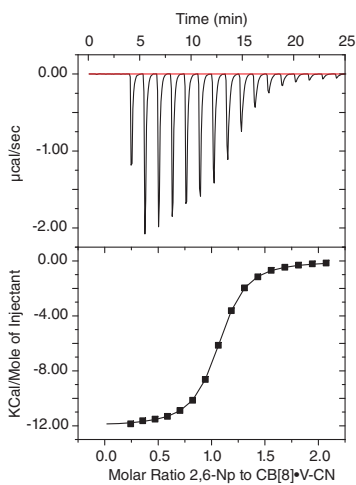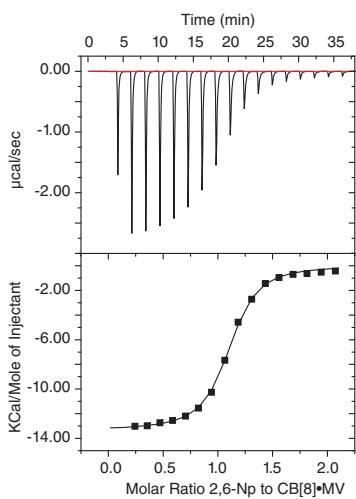

Figure S21: The binding constant of 2,6-Np with CB[8]·V-CN was determined by ITC to be (6.8 ± 0.3) x 10^5 M^{-1} in aqueous solution at 298 K.
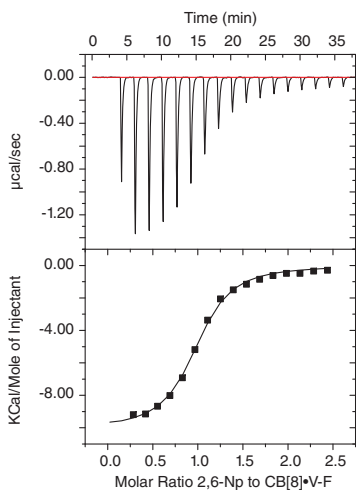
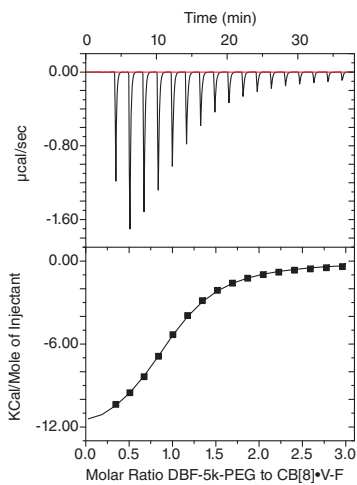Figure S22: The binding constant of 2,6-Np with CB[8]·V-F was determined by ITC to be (2.9 ± 0.3) x 10^5 M^{-1} in aqueous solution at 298 K.
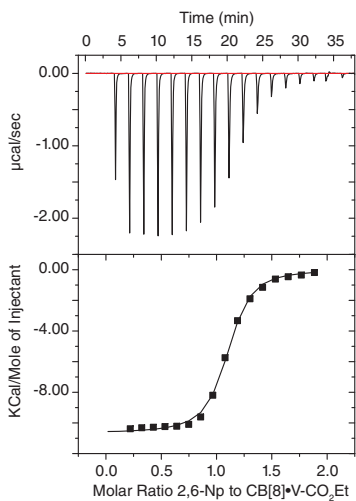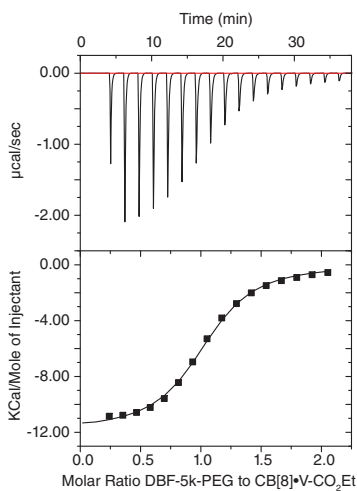

Figure S23: The binding constant of 2,6-Np with CB[8]·V-CO$_2$Et was determined by ITC to be (9.4 ± 0.3) x 10^5 M^{-1} in aqueous solution at 298 K.
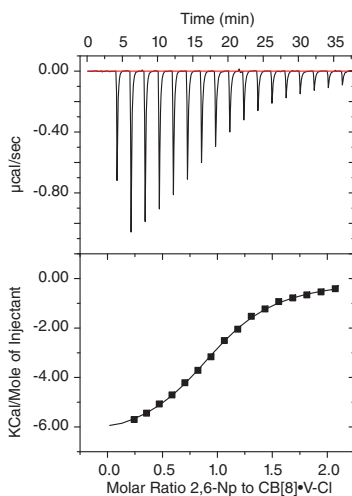
Figure S24: The binding constant of 2,6-Np with CB[8]·V-Cl was determined by ITC to be (9.3 ± 0.2) x 10^4 M^{-1} in aqueous solution at 298 K.
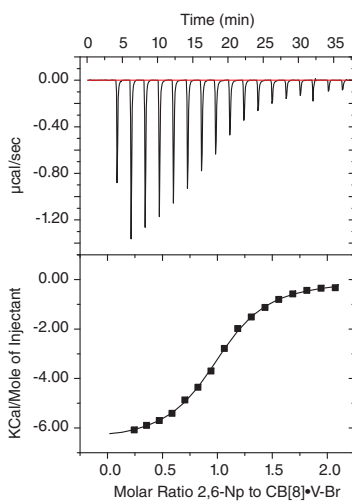
Figure S25: The binding constant of 2,6-Np with CB[8]·V-Br was determined by ITC to be (1.8 ± 0.3) x 10^5 M^{-1} in aqueous solution at 298 K.
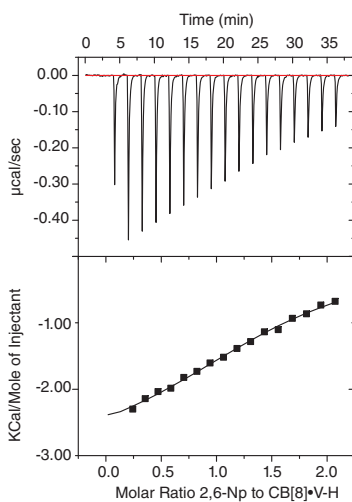
Figure S26: The binding constant of 2,6-Np with CB[8]·V-H was determined by ITC to be $(2.3\pm0.2) \times 10^4$ M^{-1} in aqueous solution at 298 K.
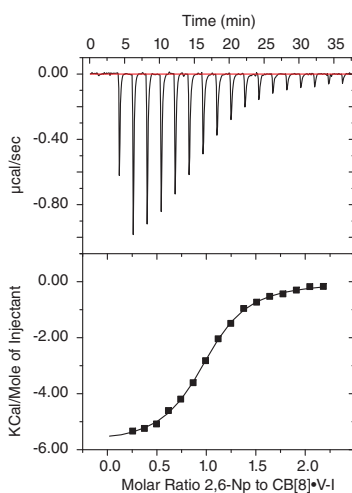
Figure S27: The binding constant of 2,6-Np with CB[8]·V-I was determined by ITC to be $(2.1\pm0.3) \times 10^5$ M^{-1} in aqueous solution at 298 K.
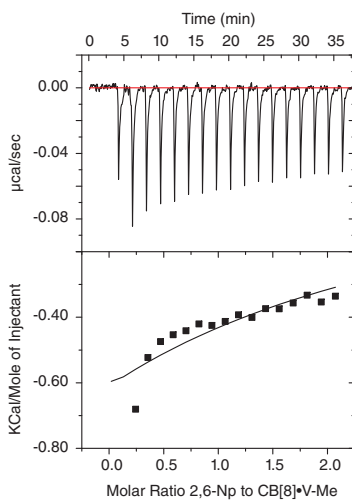
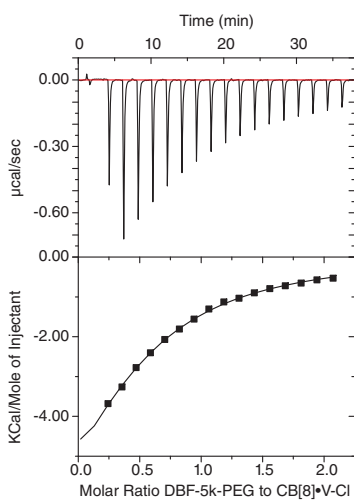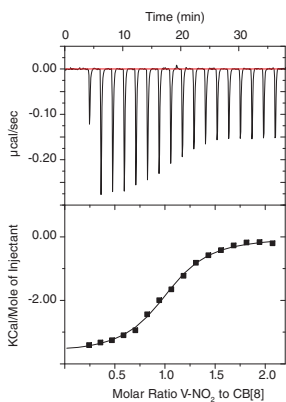Figure S28: The binding constant of 2,6-Np with CB[8]·V-Me was estimated by ITC to be $\leq 10^3$ M^{-1} in aqueous solution at 298 K.
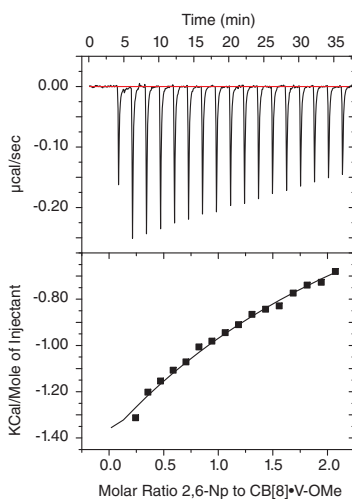
Figure S29: The binding constant of 2,6-Np with CB[8]·V-OMe was determined by ITC to be (1.3±0.3) x 10^3 M^{-1} in aqueous solution at 298 K.
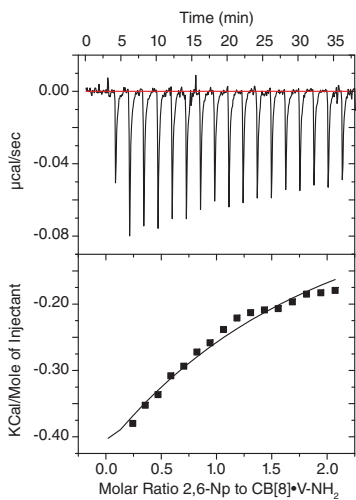
Figure S30: The binding constant of 2,6-Np with CB[8]·V-NH$_2$ was determined by ITC to be (2.9 ± 0.4) x 10^3 M^{-1} in aqueous solution at 298 K.

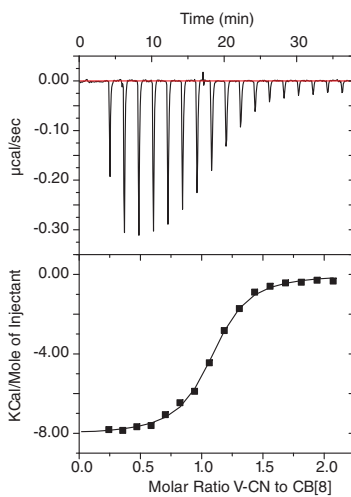

Figure S31: The binding constant of 2,6-Np with CB[8]·MV was determined by ITC to be (6.8 ± 0.3) x 10^5 M^{-1} in aqueous solution at 298 K.

# 7 ITC: $K_{aq}(2)$ determination with DBF-5k-PEG
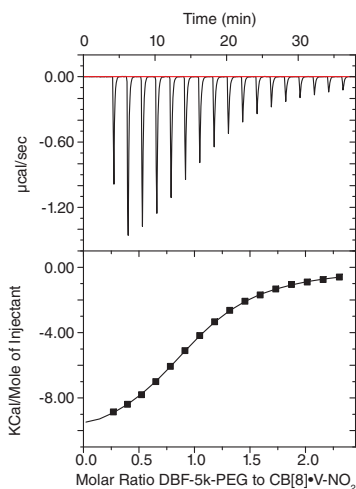
Figure S32: The binding constant of DBF-5k-PEG with CB[8]·V-NO$_2$ was determined by ITC to be (8.1±0.3) x 10^4 M^{-1} in aqueous solution at 298 K.
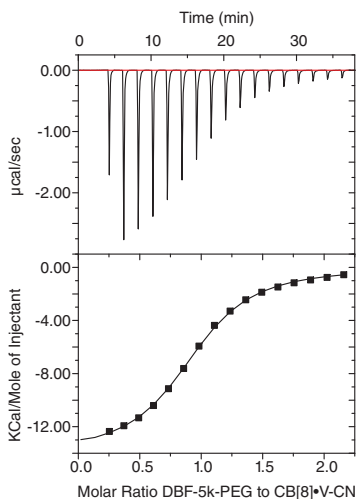
Figure S33: The binding constant of DBF-5k-PEG with CB[8]·V-CN was determined by ITC to be (1.4±0.3) x 10^5 M^{-1} in aqueous solution at 298 K.
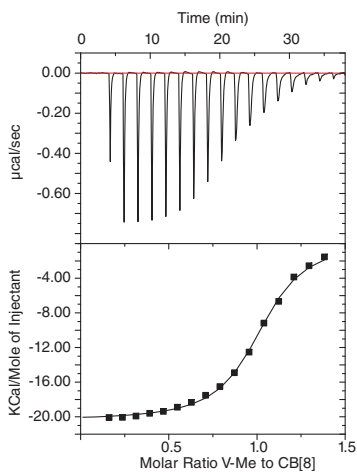
Figure S34: The binding constant of DBF-5k-PEG with CB[8]·V-F was determined by ITC to be (1.1 ± 0.3) x 10^5 M^{-1} in aqueous solution at 298 K.
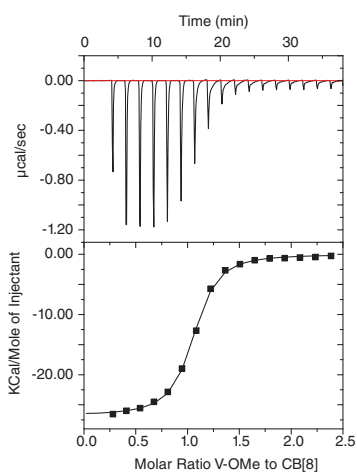

Figure S35: The binding constant of DBF-5k-PEG with CB[8]·V-CO$_2$Et was determined by ITC to be (2.2 ± 0.3) x 10^5 M^{-1} in aqueous solution at 298 K.

Figure S36: The binding constant of DBF-5k-PEG with CB[8]·V-Cl was determined by ITC to be $(1.7 \pm 0.2) \times 10^4$ M^{-1} in aqueous solution at 298 K.

8 ITC: $K_{aq}(1)$ determination

Figure S 37: The binding constant of V-NO$_2$ with CB[8] was determined by ITC to be (1.0±0.3) x 10^6 M^{-1} in aqueous solution at 298 K.

Figure S 38: The binding constant of V-CN with CB[8] was determined by ITC to be (2.5±0.3) x 10^6 M^{-1} in aqueous solution at 298 K.
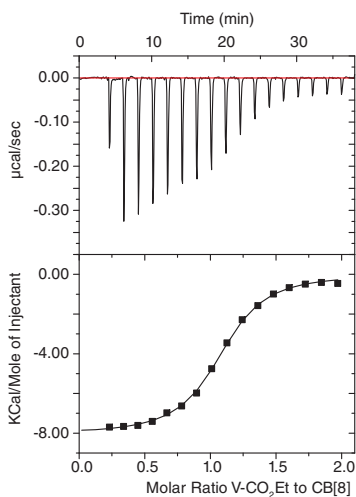
Figure S 39: The binding constant of V-CO$_2$Et with CB[8] was determined by ITC to be (1.9 ± 0.3) x 10^6 M^{-1} in aqueous solution at 298 K.
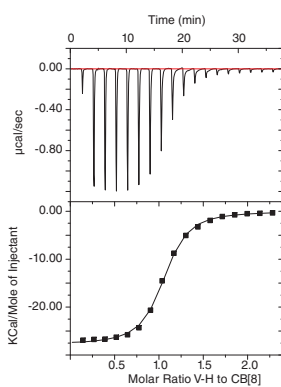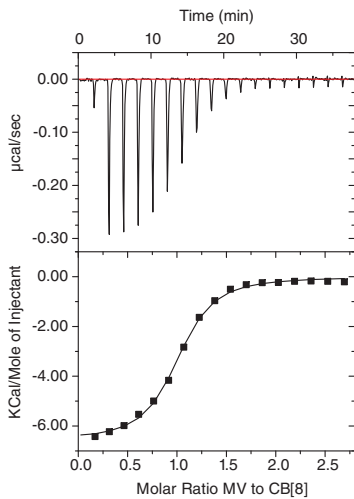

Figure S 40: The binding constant of V-H with CB[8] was determined by ITC to be (2.9 ± 0.3) x 10^6 M^{-1} in aqueous solution at 298 K.

Figure S 41: The binding constant of V-Me with CB[8] was determined by ITC to be (2.2 ± 0.3) x 10^6 M^{-1} in aqueous solution at 298 K.

Figure S 42: The binding constant of V-OMe with CB[8] was determined by ITC to be (3.9 ± 0.3) x 10^6 M^{-1} in aqueous solution at 298 K.
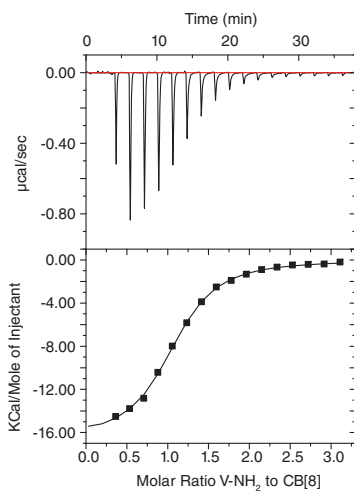
Figure S 43: The binding constant of V-NH$_2$ with CB[8] was determined by ITC to be (6.7±0.3) x 10^5 M^{-1} in aqueous solution at 298 K.

Figure S 44: The binding constant of MV with CB[8] was determined by ITC to be (1.5±0.3) x 10^6 M^{-1} in aqueous solution at 298 K.

9 ESI-MS of ternary complexes with 2,6-Np
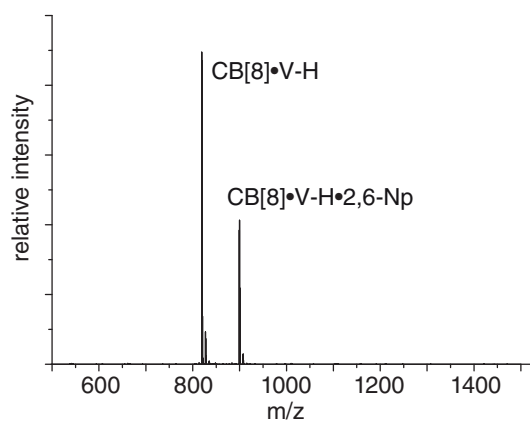
Figure S45: ES-MS spectra of CB[8]·V-H·2,6-Np (25 μM in each component).
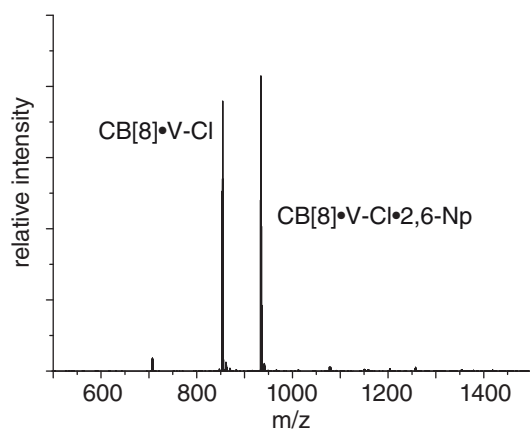
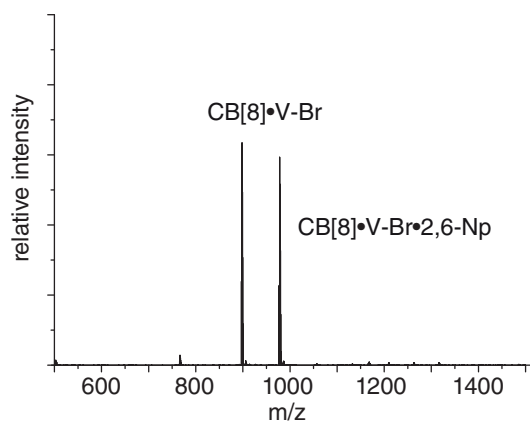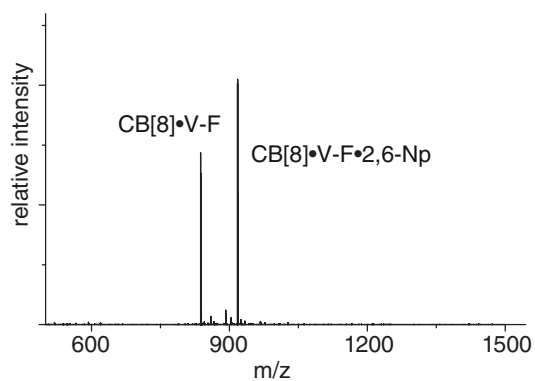Figure S46: ES-MS spectra of CB[8]·V-Cl·2,6-Np (25 μM in each component).

Figure S47: ES-MS spectra of CB[8]·V-Br·2,6-Np (25 μM in each component).

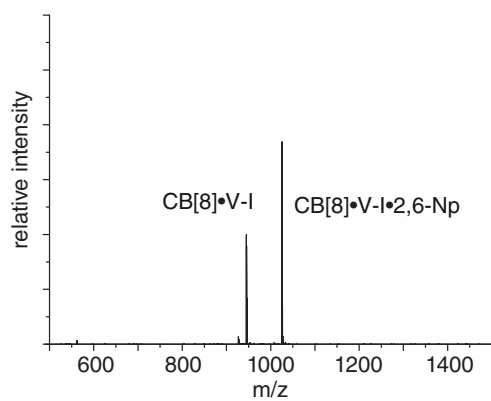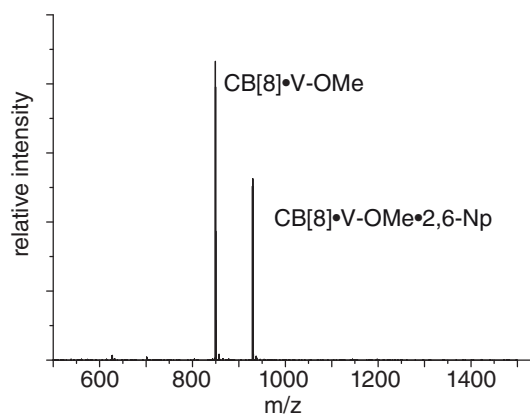Figure S48: ES-MS spectra of CB[8]·V-F·2,6-Np (25 μM in each component).

Figure S49: ES-MS spectra of CB[8]·V-I·2,6-Np (25 μM in each component).

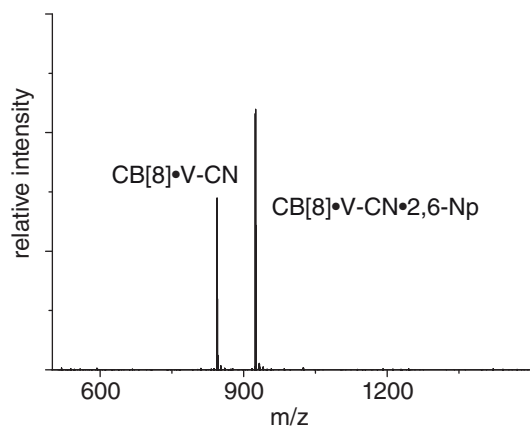Figure S50: ES-MS spectra of CB[8]·V-OMe·2,6-Np (25 μM in each component).

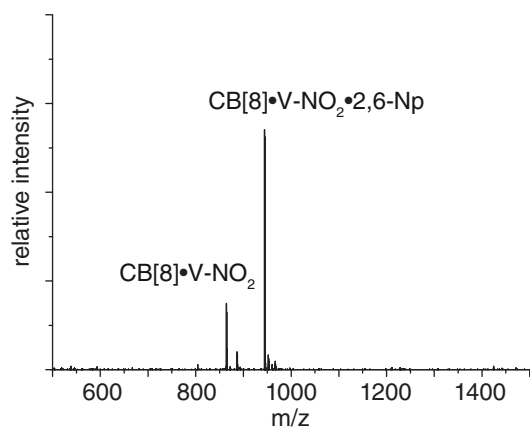Figure S51: ES-MS spectra of CB[8]·V-CN·2,6-Np (25 μM in each component).

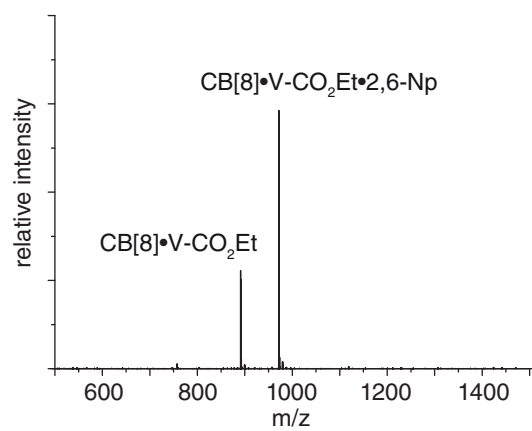Figure S52: ES-MS spectra of CB[8]·V-NO$_2$·2,6-Np (25 μM in each component).

Figure S53: ES-MS spectra of CB[8]·V-CO$_2$Et·2,6-Np (25 μM in each component).
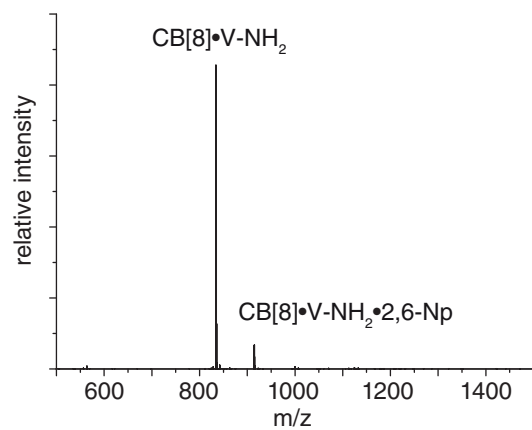
Figure S54: ES-MS spectra of CB[8]·V-NH$_2$·2,6-Np (25 μM in each component).